Correlated electronic structure, orbital-dependent correlations, and Lifshitz transition in tetragonal FeS

S. L. Skornyakov[1,2] and I. Leonov[1,3]

[1]*M. N. Miheev Institute of Metal Physics of Ural Branch of Russian Academy of Sciences, 18 S. Kovalevskaya Street, 620137 Yekaterinburg, Russia*
[2]*Ural Federal University, 620002 Yekaterinburg, Russia*
[3]*Materials Modeling and Development Laboratory, National University of Science and Technology 'MISIS', 119049 Moscow, Russia*

(Dated: May 30, 2019)

Iron-based binary chalcogenide superconductors FeSe and FeS have attracted much recent attention due to their complex orbital-selective correlations and Cooper pairing, offering the minimal model system holding the key properties to understanding the physics of high-T_c superconductors. Here, using density functional plus dynamical mean-field theory method (DFT+DMFT) with full self-consistency over the charge density, we study the effect of electronic correlations on the electronic structure, magnetic properties, orbital-dependent band renormalizations, and Fermi surface of the tetragonal phase of bulk FeS. We perform a direct structural optimization of the P_4/nmm crystal structure of paramagnetic FeS, minimizing the total energy of FeS with respect to the lattice constant a and the internal coordinate z_{S} of atom S. Our results show an anomalous sensitivity of the electronic structure and magnetic properties of FeS to fine details of its crystals structure, e.g., to a small variation of the chalcogen coordinate z_{S}. Upon expansion of the lattice volume (which can be realized, e.g., in $FeS_{1-x}Se_x$), we observe a remarkable change of the electronic structure of FeS which is associated with a complete reconstruction of the Fermi surface topology (Lifshitz transition). This behavior is ascribed to a correlation-induced shift of the Van Hove singularity associated with the Fe xy and xz/yz orbitals at the M point across the Fermi level. The Lifshitz phase transition is accompanied by a significant growth of local magnetic moments and emergence of strong orbital-selective correlations. It is seen as a pronounced anomaly ('kink') in the total energies upon expansion of the lattice, associated with a remarkable enhancement of compressibility. This behavior is accompanied by an orbital-dependent formation of local moments, a crossover from itinerant to localized orbital-selective moment behavior of the Fe $3d$ electrons. While exhibiting weak effective mass enhancement of the Fe $3d$ states $m^*/m \sim 1.3-1.4$, correlation effects reveal a strong impact on a position of the Van Hove singularity originating from the Fe xz/yz and xy orbitals at the M point, implying a complex interplay between electronic correlations and band structure effects in FeS. Our results suggest a complex interplay between electronic correlations, magnetism, and lattice degrees of freedom in FeS.

PACS numbers: 71.27.+a, 71.10.-w, 79.60.-i

I. INTRODUCTION

The discovery of unconventional superconductivity in the Fe-based pnictides and chalcogenides, with the highest transition temperature T_c up to 55 K in fluorine doped SmFeAsO and $\sim$ 109 K in a monolayer of FeSe, has attracted a lot of attention from researchers around the world in the recent past [1–3]. Similar to high-T_c cuprates, manganites or some heavy fermion compounds, the Fe-based pnictide and chalcogenide superconductors (FeSCs) are characterized by the proximity and complex interplay of various phases, including magnetism, nematicity, and crystal structure phases [4]. In fact, superconductivity in FeSCs is often found to appear in the vicinity of a magnetic phase transition and/or structural (nematic) instability, as a result of the electron/hole doping, pressure or other means suppression of long-range, single-stripe antiferromagnetic (AFM) order with a wave vector $Q_m = (\pi, \pi)$ [5]. The Fermi surface topology of FeSCs is characterized by an in-plane nesting wave vector (π, π), consistent with $s_\pm$ pairing symmetry [6, 7]. Moreover, experimental studies of the spin excitation spectra of both pnictides and chalcogenides show an enhancement of short-range AFM spin fluctuations at a vector (π, π) near the T_c [8]. This behavior has been regarded as evidence for the importance of spin fluctuations in the pairing of electrons in FeSCs.

Among various chemical compositions of FeSCs much attention has been paid to the binary chalcogenide compounds, the so-called '11' family of FeSCs, FeX with X=Se, Te, and S [4, 9, 10]. Besides their structural simplicity, the '11' FeSCs offer the minimal model system holding the key properties to understanding the physics of high-T_c superconductors in general. Iron selenide FeSe is a particularly fascinating representative of the '11' FeSCs [4, 9, 11, 12]. Unlike the iron pnictides, FeSe lacks long range magnetic order in spite of a similar structural behavior and extended nematic (orthorhombic) phase below 90 K [4, 13]. In fact, FeSe has been found to become superconducting below $T_c \sim 8$ K close to its stoichiometric composition [14]. Superconductivity in FeSe is highly tunable, with the superconducting transition tempera-

ture ranging from $T_c \sim 8$ K in bulk single crystals at ambient pressure to ~ 40 K under pressure (of ~ 6 GPa) or in intercalated systems, to ~ 14 K upon isoelectronic substitution of Se with Te (corresponding to a negative chemical pressure, i.e., lattice expansion) and to $\sim$ 65–109 K in thin films [3, 15–18]. While FeSe shows no antiferromagnetically ordered phase at ambient pressure down to the lowest temperatures, static magnetism (most likely) of the (π, π) AFM stripe-type emerges upon compression above ~ 1 GPa [8]. Moreover, a double-stripe $(\pi, 0)$-type magnetically ordered phase appears upon expansion of the lattice caused by an isoelectronic substation of Se with Te, in FeTe [19]. The (π, π) to $(\pi, 0)$ crossover in magnetic correlations can be attributed to a Lifshitz transition of the electronic band structure of Fe(Se,Te), accompanied by a remarkable increase of local magnetic moments and an enhancement of electronic compressibility at the transition point [20–22]. This behavior was ascribed to, e.g., a correlation-induced shift of the Van Hove singularity associated with the Fe xy and xz/yz orbitals at the Brillouin zone M point across the Fermi level [20–22]. Under pressure, T_c in FeSe increases dramatically to a maximum of ~ 37 K at about 6 GPa [16, 17]. By contrast, substitution of Se for S, which constitutes a positive chemical pressure on FeSe, leads to a reduction of the degree of (π, π) nesting, resulting in a decrease of T_c [23]. The latter is presumably connected with suppression of spin fluctuations, resulting in a lowering of the critical temperature in $FeSe_{1-x}S_x$ series [22, 24].

Being isoelectronic and isostructural counterpart of FeSe, the tetragonal FeS has attracted a lot of attention from both theory and experiment as a promising model system to study the underlying mechanisms (e.g., the interplay of magnetism and structural parameters) of superconductivity in FeSCs [25]. In contrast to FeSe and the majority of FeSCs, FeS does not reveal a structural transition from the tetragonal to orthorombic structural phase (i.e., it exhibits no nematic order) down to the lowest temperatures [4, 24, 26]. Moreover, superconducting (SC) properties of FeS display a delicate interplay with the lattice. The T_c is first found to decrease under pressure. However, upon further compression, it is followed by a reemergence of SC with formation of a second SC dome on the phase diagram [27, 28]. This behavior can be attributed to a Lifshitz transition which adds a hole pocket to the Fermi surface (FS) [29]. From angle-resolved photoemission experiments (ARPES) and electronic structure calculations the Fermi surface of FeS resembles that of FeSe [24, 30, 31]. It features two electron-like pockets at the tetragonal Brillouin zone M points and two hole-like pockets centered at the Γ point, showing a moderate dispersion along k_z. However, at ambient pressure the third hole-like pocket at Γ in FeS is not observed [24, 31]. In addition, ARPES shows that the increase of S content in the solid solution $FeSe_{1-x}S_x$ leads to an increase of the size of the FS, accompanied with a reduction of the degree of (π, π) in-plane nesting [23, 24]. The latter suggests damping of spin fluctuations in FeS compared to those in FeSe. Photoemission and ARPES measurements of the electronic properties of FeS reveal a sufficient narrowing of the Fe $3d$ bandwidth as compared to band structure calculations [30]. However, an orbital-dependent band renormalization of the quasiparticle mass is weaker than that in FeSe and is only about $\sim$ 1.5–2, implying a remarkably weaker strength of correlation effects in FeS [24, 32]. In this context it is interesting to note the possible importance of electron-phonon coupling in FeS [33].

The most advanced theoretical methods for calculation of the electronic properties of strongly correlated materials, such as the density functional theory plus dynamical mean theory approach (DFT+DMFT) have shown to provide a good description of the electronic structure of FeSCs [34–36]. For FeSCs DFT+DMFT calculations reveal significant correlation effects with orbital-dependent strength and character, revealing the importance of the Hund's rule coupling induced many-body correlations [20–22, 32, 36–39]. This leads to substantial differences in quasiparticle weights and orbital selectivity of electronic correlations, suggesting that the Cooper pairing can also become orbital-selective, with a highly anisotropic superconducting gap [11, 12]. Moreover, such DFT+DMFT calculations indicate a positive correlation of the enhancement of the T_c with the correlation-induced increase of the electronic compressibility, suggesting that the system is at the frontier of the normal-to-Hund's metal crossover [20–22, 39]. Applications of DFT+DMFT to the equilibrium phase of FeS and FeSe have shown that the electronic properties of FeS share many similarities with those of FeSe [32]. In agreement with ARPES measurements, the DFT+DMFT calculations suggest weaker orbital-dependent band renormalizations in FeS [24, 32]. In FeSe correlations are strong enough to induce a transfer of the spectral weight and form the lower Hubbard band whereas the existence of the low-energy correlation-induced satellite in tetragonal FeS remains an open question [38, 40].

As already discussed in many respects for FeSCs, the crystal structure effects (variation of the lattice under pressure and/or chemical substitutions) show a strong impact on the electronic properties and magnetic fluctuation spectrum of FeSCs, implying a complex coupling between the magnetic and structural properties [4]. It often results in a significant enhancement of the T_c's upon a moderate variation of crystal structure parameters of FeSCs. This behavior still needs to be understood on a microscopic level that drives much attention to the physical properties of the '11' FeSCs. In this respect FeS, a superconducting system exhibiting no nematic ordering, offers new perspectives to study the coupling between the magnetic and structural properties in FeSCs.

In this paper, we study the interplay of the electronic structure, magnetic properties, and the Fermi surface topology in the tetragonal (space group P_4/nmm) paramagnetic FeS upon variation of its crystal structure.

In particular, by employing the DFT+DMFT method [34, 35] we study the effect of the lattice structure, e.g., a change of the lattice volume and chalcogen coordinate z_S on the electronic properties, magnetic correlations, and the Fermi surface of FeS. Our results reveal the importance of electronic correlations for the electronic properties and structural optimization of FeS. For examples, we observe a strong impact of correlation effects on a position of the Van Hove singularity originating from the the Fe xz/yz and xy orbitals at the M point. We show that the internal parameter z_S plays a key role for understanding the physical properties of FeS upon expansion of the lattice. Upon lattice expansion FeS is found to exhibit a structural collapsed-tetragonal to tetragonal phase transition, accompanied by a significant increase of local magnetic moments and an emergence of strong orbital-selective correlations near the transition point. The phase transition results in a remarkable increase of the electronic compressibility and is associated with a topological change of the Fermi surface (Lifshitz transition). The latter is accompanied by a crossover from itinerant to localized orbital-selective moment behavior. Our results clearly demonstrate the crucial importance of orbital-selective correlations for a realistic description of the electronic and lattice properties of FeS.

The paper is organized as follows. In Sec. II we describe the technical details of our DFT+DMFT calculations. In Sec. III A we present results for crystal structure optimization of FeS, focusing on the evolution of its electronic structure and local magnetic moments. Spectral properties and orbital-selective renormalizations of the Fe $3d$ states of FeS are discussed in Sec. III B. Our results for the evolution of the Fermi surface and spin susceptibility upon variation of the crystal structure parameters of FeS are shown in Sec. III C and D, respectively. Finally, the results are summarized in Sec. IV.

II. METHOD

Here, we study the effect of electronic correlation on the electronic structure, magnetic correlations, and crystal structure properties of tetragonal FeS (space group P_4/nmm) using the state-of-the-art fully self-consistent in charge density DFT+DMFT method [34, 35]. We perform a direct structural optimization of the tetragonal P_4/nmm unit cell of FeS, minimizing the total energy of FeS with respect to the lattice constant a and the internal coordinate of sulphur z_S (z_S is proportional to the height of S relative to the basal Fe plane). In these calculations, the c/a ratio of the tetragonal unit cell was fixed to its experimental value $c/a = 1.367$ (at ambient pressure). To compute pressure, equilibrium lattice volume and bulk modulus we fit the calculated total energies using the third-order Birch-Murnaghan equation of state [41]. We note that the DFT+DMFT results exhibit a clear anomaly in the total energy behavior. Therefore we fit the equation of states separately for the low- and high-volume regions.

We have employed the DFT+DMFT approach implemented within the plane-wave pseudopotential formalism with generalized gradient approximation (GGA) for the DFT exchange-correlation potential [42]. The DMFT equations are solved in a basis set of the Wannier Fe $3d$ and O $2p$ orbitals. The latter are constructed using the atomic-centered symmetry-constrained Wannier functions defined over the full energy range spanned by the Fe $3d$ and the S $4p$ bands [43]. We solve the realistic many-body problem using the continuous-time hybridization-expansion (segment) quantum Monte Carlo algorithm [44]. The calculations are performed in the paramagnetic state at an electronic temperature $T = 290$ K. The Coulomb interaction has been treated in the density-density approximation with the average Hubbard interaction $U = 3.5$ eV and Hund's exchange $J = 0.85$ eV for the Fe $3d$ shell, as estimated previously [36]. The interaction parameters U and J are assumed to remain constant upon variations of the lattice. The spin-orbit coupling was neglected in our calculations. To account for the electronic interaction already described by DFT, we employ the fully localized double counting correction, evaluated from the self-consistently determined local occupations. Spectral properties and renormalizations of the effective electron mass of the Fe $3d$ orbitals are obtained from the real-axis self-energy $\hat{\Sigma}(\omega)$ computed using the Padé analytical continuation procedure [45].

To quantify a degree of localization of the Fe $3d$ electrons of FeS upon variation of the lattice we compute the local spin-spin correlation function $\chi(\tau) = \langle \hat{m}_z(\tau)\hat{m}_z(0)\rangle$ within DMFT, where $\hat{m}_z(\tau)$ is the instantaneous magnetization on the Fe $3d$ state at the imaginary time τ. The evolution of magnetic correlations and possible magnetic instabilities of FeS upon variation of the lattice is analyzed by calculating the momentum-resolved static susceptibility in the particle-hole bubble approximation:

$$\chi(\mathbf{q}) = -k_B T \sum_{\mathbf{k}, i\omega_n} \mathrm{Tr}\hat{G}(\mathbf{k}, i\omega_n)\hat{G}(\mathbf{k}+\mathbf{q}, i\omega_n), \qquad (1)$$

where $\hat{G}(\mathbf{k}, i\omega_n)$ is the interacting lattice Greens function evaluated within DFT+DMFT, T is the electronic temperature, and ω_n is the fermionic Matsubara frequencies.

III. RESULTS

A. Structural optimization and local magnetic moments

We start by performing a direct structural optimization of the P_4/nmm crystal structure of paramagnetic FeS. To this end, we minimize the total energy of FeS with respect to the lattice constant a and the internal coordinate z_S of atom S using the DFT+DMFT method

with the average Coulomb interaction $U = 3.5$ eV and Hunds exchange $J = 0.85$ eV for the Fe $3d$ shell. In Fig. 1 we compare our DFT+DMFT results with the results of the nonmagnetic GGA (nm-GGA) calculations (i.e., with the noninteracting case of $U = 0$ eV and $J = 0$ eV). Our nm-GGA results for the total energy show a typical parabolic-like behavior with the equilibrium lattice constant $a = 6.84$ a.u. and the fractional coordinate $z_S = 0.241$ ($a = 6.78$ a.u. for the fixed $z_S = 0.252$). The calculated a and z_S crystal structure parameters are by $\sim 2\%$ and 4% smaller than those in the experiment, respectively. The calculated bulk modulus is found to depend very sensitively on the coordinate z_S (i.e., whether z_S is optimized or not). In particular, the bulk modulus computed from a fit of the DFT total energy to the third-order Birch-Murnaghan equation of state for the case with z_S fixed to its experimental value $z_S = 0.252$ is $K \sim 137$ GPa. The bulk modulus pressure derivative is $K' \equiv dK/dP = 4.8$. On the other hand, structural optimization of FeS within nm-GGA with respect to both the lattice constant a and coordinate z_S gives $K = 67$ GPa. We note however that this value is still significantly higher (by about two times) than available experimental estimates for nanocrystalline tetragonal FeS (~ 30 GPa) [46]. Interestingly, for the parent compound FeSe, which is isoelectronic and isostructural to FeS, experimental studies give $K \sim 31 - 33$ GPa [47].

Structural optimization of the lattice parameters of paramagnetic FeS within DFT+DMFT gives an overall improvement for the calculated crystal structure parameters with respect to the non-interacting nm-GGA results. Our results for the lattice constant $a \sim 6.93$ a.u. (less than about 1% off the experimental value) and the internal coordinate $z_S = 0.247$ (smaller by $\sim$2 %) are in good agreement with available experiments. For the bulk modulus we obtain $K = 106$ GPa (for z_S fixed to its experimental value), while simultaneous optimization of a and z_S within DFT+DMFT gives a significantly softer crystal lattice with $K \sim 50$ GPa. The latter estimate is in reasonable agreement with the experimental bulk modulus of nanocrystalline tetragonal FeS (~ 30 GPa) and with the bulk modulus of FeSe (31–33 GPa) [47, 48]. We note that the calculated height of the chalcogen atom, sulphur in FeS, relative to the basal Fe plane of 2.332 a.u. ($z_S = 0.247$) is by $\sim 15\%$ smaller than that in the parent compound FeSe (2.729 a.u.), in agreement with the experiment. The calculated instantaneous local magnetic moment is $\sqrt{\langle \hat{m}_z^2 \rangle} = 1.75\ \mu_B$ (corresponding to the fluctuating local moment of $M_{loc} = 0.40\ \mu_B$, evaluated as $M_{loc} = (k_B T \int_0^{1/k_B T} d\tau \langle \hat{m}_z(\tau) \hat{m}_z(0) \rangle)^{1/2}$, where T is the temperature) at ambient pressure. The calculated value of $\sqrt{\langle \hat{m}_z^2 \rangle}$ is by ~ 8 % smaller as compared to that obtained for paramagnetic FeSe. Clearly, it is the inclusion of the local Coulomb interaction that provides an overall improved description of the properties of FeS compared to the nm-GGA results.

Our results for the calculated crystal structure and electronic structure parameters of FeS are summarized in Table I. We find that the calculated crystal lattice parameters of FeS are in overall good agreement with recent experimental data. Most importantly, the DFT+DMFT calculations predict an isostructural phase transition which is accompanied by a substantial increase of the local magnetic moments $\sqrt{\langle \hat{m}_z^2 \rangle}$ (a formation of local moments) upon expansion of the lattice of FeS, i.e., under a "negative" (chemical) compression. Indeed, our calculations reveal a pronounced anomaly in the total energy upon expansion of the lattice, associated with a remarkable enhancement of electronic compressibility near $a \sim 7.5$–7.7 a.u. ($a \sim 7.5$ a.u. for fixed z_S and ~ 7.7 a.u. upon simultaneous optimization of a and z_S, respectively) [49]. Moreover, the instantaneous local moments which are $\sqrt{\langle \hat{m}_z^2 \rangle} \sim 1.75\ \mu_B$ at ambient conditions are found to increase to 3.36 μ_B and 2.86 μ_B at $a = 8.2$ a.u., respectively (see lower panel of Fig. 1).

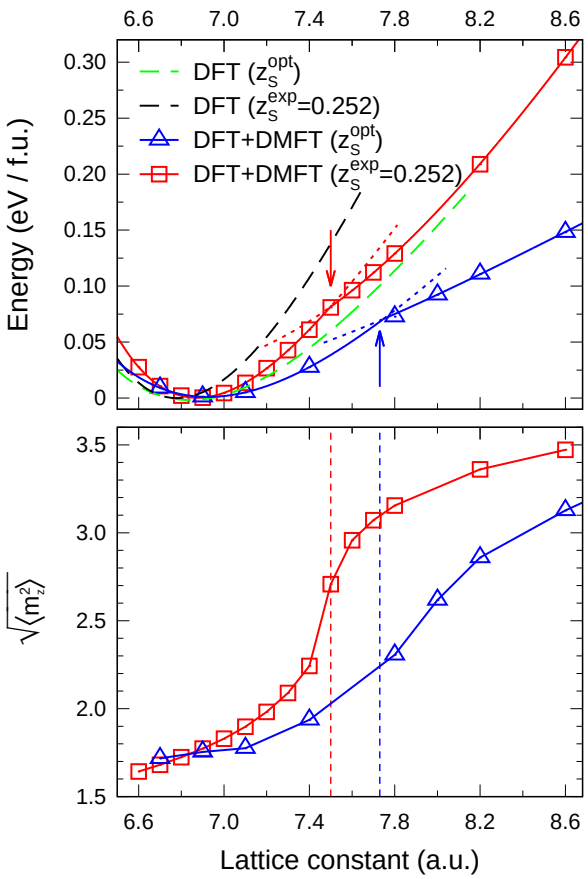

FIG. 1: (Color online). Total energy (upper panel) and instantaneous local moment $\sqrt{\langle \hat{m}_z^2 \rangle}$ (lower panel) of paramagnetic FeS as a function of the lattice constant calculated by the charge self-consistent DFT+DMFT method at $T = 290$ K for the experimental (z_S^{exp}) and optimized (z_S^{opt}) internal position of sulphur. The results for the total energy obtained within nonmagnetic GGA are shown in the upper panel for comparison (dashed curves). The phase transition point is indicated by arrows (upper panel) and by vertical dashed lines (lower panel).

Interestingly, structural optimization of both a and z_S results in a smooth evolution of the local moments as a function of volume, while the lattice anomaly shifts to a higher volume with $a \sim 7.8$ a.u.. We note that similar anomalous behavior of the lattice structure and local magnetic moments upon lattice expansion has been found in the parent system FeSe [20–22]. By analogy with FeSe, we interpret this behavior of FeS as a transition from a collapsed-tetragonal (equilibrium volume) to tetragonal (expanded volume) phase which occurs upon expansion of the lattice volume. The transition is of first order, occurs under a negative pressure of above 15 GPa (in practice it can be realized, e.g., by substituting S with Se), which is as twice as that found in FeSe. The expanded-volume phase has a significantly smaller bulk modulus of ~ 27 GPa.

Our results show that the phase transition is accompanied by an increase of the lattice constant from $a = 7.3$ a.u. to 7.8 a.u. (with fixed $z_S = 0.252$), as obtained from a common tangent construction for the energy-volume dependence. The latter corresponds to a large increase of the lattice volume by $\Delta V/V \sim 18$ %. We note that optimization of z_S further lowers the energy of the expanded-volume phase and results in a significant extension of the transition region. This implies a significant variation of the z_S value at the transition. The phase transition spans the range from $a \sim 7.4$ a.u. to about ~ 8.6 a.u., implying the importance of optimization of all crystal structure parameters, including c/a, for the expanded-volume phase of FeS. Moreover, similarly to FeSe this anomaly of the crystal structure of FeS is not observed in spin-polarized DFT calculations for the $(\pi, 0)$ and (π, π) antiferromagnetic ordering of Fe moments, demonstrating the importance of electronic correlations in FeS [50].

B. Spectral properties and band renormalizations

Next, we discuss the spectral properties of paramagnetic FeS. In Fig. 2 we show the spectral functions of FeS calculated for the equilibrium structure and for the high-volume phase ($a = 8.20$ a.u. for the fixed $z_S = 0.252$ and $a = 8.60$ a.u. for the optimized $z_S = 0.127$). Our results for the electronic band structure of FeS obtained within

TABLE I: Calculated equilibrium structural parameters of FeS and the position of Van Hove singularity $E_{\rm VHS}^{\rm DMFT}$ at the M point (relative to the Fermi energy) obtained by DFT+DMFT at $T = 290$ K in comparison to the results for FeSe [22]. Here, $h_{\rm ch}$ is the height of a chalcogen atom (ch=S, Se) above the basal Fe plane and $E_{\rm VHS}^{\rm GGA}$ is the position of VHS in nm-GGA.

	$E_{\rm VHS}^{\rm GGA}$ (eV)	$E_{\rm VHS}^{\rm DMFT}$ (eV)	$z_{\rm ch}$	$h_{\rm ch}$ (a.u.)	c/a
FeS	−0.35	−0.21	0.247	2.332	1.367
FeSe	−0.25	−0.12	0.261	2.729	1.494

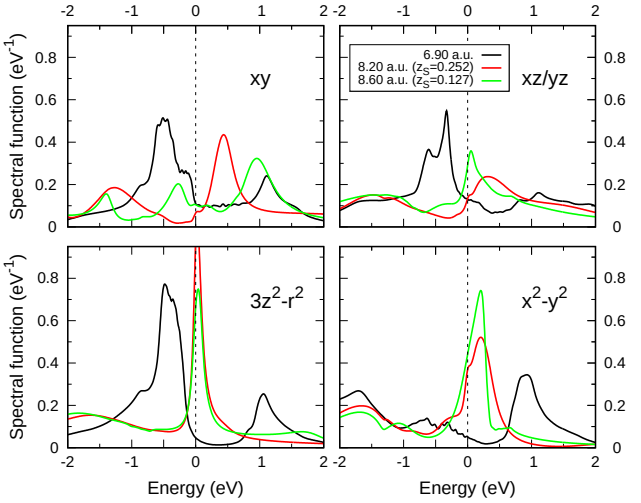

FIG. 2: (Color online). Orbitally-resolved Fe $3d$ spectral functions of FeS computed by DFT+DMFT at $T = 290$ K for the equilibrium lattice volume (black) and those in the expanded-volume phase with experimental $z_S = 0.252$ (red) and optimized $z_S = 0.127$ (green). The Fermi energy is shown by a vertical dashed line ($E_F = 0$ eV).

DFT+DMFT for the calculated equilibrium structural parameters $a = 6.90$ a.u. and $z_S = 0.252$ for are shown in Fig. 3. We notice that the spectral functions of FeS are qualitatively similar to those calculated earlier for the parent compound FeSe. Moreover, in qualitative agreement with FeSe, the Fe xy and xz/yz spectral functions exhibit a well-defined quasiparticle peak (QP) located below the Fermi level at about -0.32 eV. Our analysis of the correlated band structure of FeS suggests that this peak is originating from the Van Hove singularity (VHS) of the xy and xz/yz bands located below E_F at about -0.21 eV at the M point. In addition, the spectral functions for the t_2 orbitals of FeS exhibit a broad feature at ~ -1.5 eV, associated with the lower Hubbard band. For comparison, the DFT+DMFT calculations for FeSe place the QP associated with the Fe xy and xz/yz VHS at ~ -0.2 eV below the Fermi level.

We find a substantial renormalization of the Fe $3d$ bands with respect to the nm-GGA results, which is however sufficiently weaker than in FeSe. In fact, our results for the orbital-selective renormalization of the Fe $3d$ states evaluated from $m^*/m = 1 - \partial\Sigma(\omega)/\partial\omega|_{\omega\to 0}$ (here, $\Sigma(\omega)$ is the self-energy in the real-frequency domain computed by employing Padé approximants [45]) exhibit a rather weak enhancement of m^*/m, ranging in 1.3–1.4 (see Table II). This implies that at ambient conditions FeS is a weakly correlated system with small orbital-selective renormalizations. The Fe t_2 states are being renormalized by about 1% stronger than the e states. We note that the DFT+DMFT results for FeSe in the vicinity of the equilibrium lattice volume give m^*/m lying in the range 1.5–2. In accordance with this, our DFT+DMFT calculations show that the Fe $3d$ band-

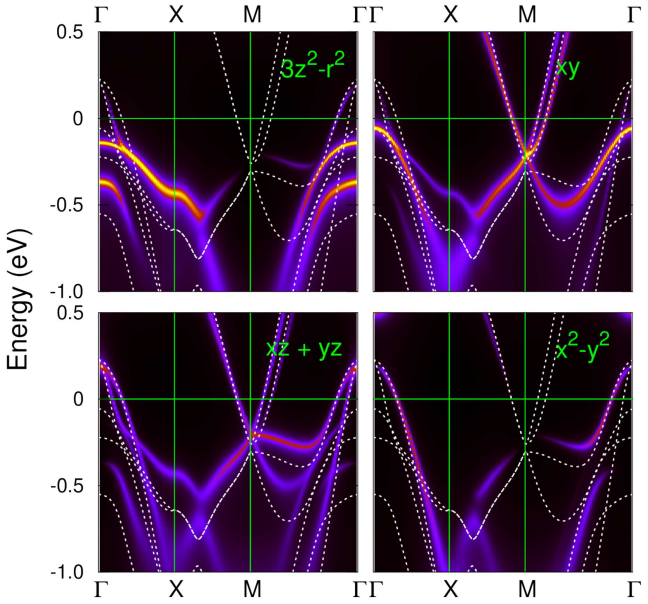

FIG. 3: (Color online). Band structure of FeS along the Γ-X-M-Γ path obtained by DFT+DMFT at ambient pressure ($a = 6.90$ a.u., $z_S = 0.252$) for $T = 290$ K. The dashed curves show the nm-GGA results.

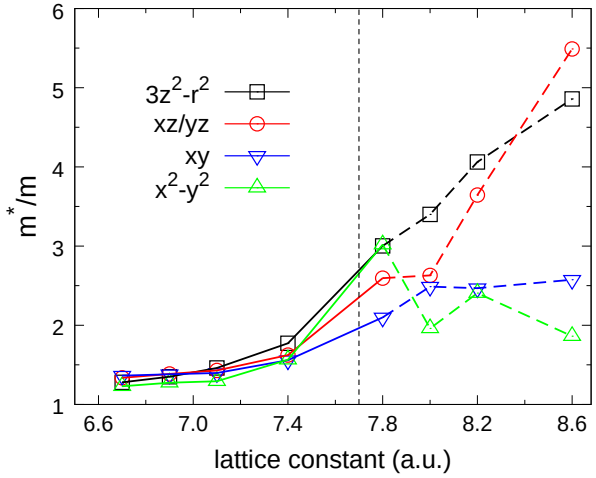

FIG. 4: (Color online). Orbitally-resolved quasiparticle mass enhancement m^*/m of the Fe $3d$ states in paramagnetic FeS as a function of lattice constant calculated by DFT+DMFT with optimized z_S at $T = 290$ K. The phase transition point is indicated by a vertical dashed line.

width of FeS is by $\sim 10\%$ larger as compared to that of FeSe, implying overall weaker correlation effects in FeS. Nonetheless, we point out that the effect of correlations on the electronic structure of FeS is non-negligible, resulting in a significant shift of the quasiparticle bands in the vicinity of the Fermi level. In particular, we observe a remarkable shift of the Fe xz/yz and xy VHS at the M point towards the Fermi level by about 40%, caused by correlation effects. The VHS shifts from -0.35 eV in the nm-GGA to -0.21 eV below the Fermi energy in the DFT+DMFT calculation (see Fig. 3). Interestingly, in FeSe the correlation-induced shift of VHS towards the Fermi energy is even stronger. In particular, the VHS shifts from -0.24 eV (in nm-GGA) to -0.12 eV in the equilibrium phase of FeSe.

In addition, we notice a remarkable correlation between the position of VHS and the strength of electronic correlation effects in FeSe and FeS (see Fig. 4 for FeS and Fig. 7 in Ref. [21] for FeSe). In fact, our results show that both FeS and FeS exhibit a significant orbital-dependent increase of m^*/m to ~ 3 upon the VHS approaching the Fermi level (upon expansion of the lattice). While considering a 'blue-red shift' problem in FeSCs (an inappropriate shifting upward of the electron bands at the M point and downward of the holelike bands at the Γ point, resulting in a shift of VHS away from E_F) this rises important question about the interplay of VHS and correlation effects in FeSCs [51].

Upon expansion of the lattice, we find a substantial redistribution of the Fe $3d$ spectral weight near the Fermi energy. We note that the overall change of the spectral function shape upon expansion of the lattice agrees with the evolution of photoemission spectra of Fe(Se,Te) obtained upon substitution of Se with Te [52]. We observe that a substantial part of the spectral weight of the Fe xz/yz and xy orbitals in the vicinity of E_F is pushed from below to above the Fermi level. In particular, the QP peak associated with the VHS at -0.23 eV below the Fermi level in the equilibrium volume phase is absent for larger volumes. The $x^2 - y^2$ spectral weight shifts in the opposite direction, towards E_F, from ~ 1 eV to 0.25 eV above E_F. The $3z^2 - r^2$ states form a quasiparticle peak near the Fermi level in the high-volume phase.

The spectral weight transfer is accompanied by a remarkable orbital-selective renormalization of the Fe $3d$ bands. In fact, the effective mass of the Fe t_2 states increases to ~ 5.49 for the xz/yz and 2.58 for the xy orbitals, i.e., almost by about 4 times and by 2 times with respect to the equilibrium values (see Table II). Moreover, we find that the effective mass of the Fe $3d$ states depends very sensitively on the lattice constant a and coordinate z_S. For example, our results show a significant change of m^*/m for the xz/yz and xy orbitals, from $m^*/m = 7.04$ and 6.94 for $z_S = 0.127$ to 3.64 and 2.47 for $z_S = 0.157$, respectively. In addition, we find a significant renormalization of the $3z^2 - r^2$ orbitals, from $m^*/m \sim 1.35$ for the equilibrium lattice to 4.86 for the high-volume phase with $a = 8.60$ a.u. and $z_S = 0.127$. In Table II we also present our results for the orbital-dependent occupations of the Fe $3d$ states. Interestingly, the calculated orbital-selective renormalization of the Fe $3d$ states is accompanied by a change of the corresponding Fe $3d$ occupancies towards the half-filled state.

C. Fermi surface and Lifshitz transition

To understand the effects of lattice expansion and electronic correlations in more detail, we analyze the **k**-resolved spectral properties of FeS. For this purpose, we determine the poles of the DFT+DMFT lattice Green's function $\hat{G}(\mathbf{k},\omega)$ (evaluated using $\hat{\Sigma}(\omega)$) and compute the momentum-resolved spectral function $A(\mathbf{k},\omega) = -\frac{1}{\pi}\mathrm{Tr}\hat{G}(\mathbf{k},\omega)$. The former allows us to visualize the quasiparticle Fermi surface. On the other hand, the spectral function $A(\mathbf{k},\omega)$ can be used to analyze the spectral weight at E_F. In Figs. 5 and 6 we show our results for the spectral weight at the Fermi energy (top row in Figs. 5 and 6) and the quasiparticle Fermi surface (bottom) obtained by DFT+DMFT for the different structural parameters a and z_S. For the equilibrium lattice parameters, the Fermi surface exhibits two hole sheets centered at the Γ-Z direction and two FSs at each of the four corners (M-Z direction) of the tetragonal Brillouin zone (BZ). The cross-section area of the corner FSs shows a strong dependence on k_z, reaching its minimum for $k_z = 0$ and a maximum at the BZ boundary. The Fermi surface of the outer hole cylinder (mostly originating from a combination of the Fe xz/yz and x^2-y^2 states) is almost parallel to the Γ-Z direction, i.e., two-dimensional. By contrast, the inner FS pocket has a less pronounced 2D character with a sufficient variation of its cross-section along k_z. Our results for the spectral weight show coherent FSs, implying a small damping of quasiparticles in the equilibrium phase. This is consistent with a weak renormalization of the Fe $3d$ states in the equilibrium phase.

Upon expansion of the lattice, we observe an entire reconstruction of the Fermi surface topology (Lifshitz transition) of FeS. With fixed $z_\mathrm{S} = 0.252$, the FSs at the corners of the BZ vanish, while those centered at Γ-Z change their shape and significantly increase in size. In particular, now there are two hole-like quasi-2D FSs at Γ-Z. The shape of the outer sheet is cylinder-like at the zone boundary $k_z = \pi$, with insufficient expansion along the (π,π,k_z) diagonals near $k_z = 0$ (see Fig. 5). The inner FS is almost parallel to Γ-Z and shows a cross-like cross-section at $k_z = 0$. We note that in the expanded-volume phase the spectral weight distribution at the E_F is highly incoherent. This is mostly due to the inner FS pocket and is seen as four spots at $(\pi,0)$. The incoherent spectral weight at E_F implies a stronger damping of quasiparticles in the high-volume phase, in agreement with a larger band renormalization m^*/m. In this case, the overall evolution of the FS shape resembles that obtained within DFT+DMFT for FeSe [20, 21].

TABLE II: Orbitally-resolved enhancement of the effective mass m^*/m (top) and occupations of the Fe $3d$ states per spin (bottom) of FeS for different lattice parameters as computed by the charge self-consistent DFT+DMFT method at T = 290 K.

Structural parameters		m^*/m			
a (a.u.)	z_S	$3z^2-r^2$	xz/yz	xy	x^2-y^2
6.90	0.252	1.36	1.41	1.42	1.29
8.20	0.252	3.65	7.04	6.94	2.50
8.20	0.157	4.06	3.64	2.47	2.41
8.60	0.127	4.86	5.49	2.58	1.86
		occupancies (per spin)			
6.90	0.252	0.81	0.69	0.72	0.73
8.20	0.252	0.74	0.61	0.60	0.76
8.20	0.157	0.69	0.69	0.63	0.73
8.60	0.127	0.70	0.67	0.62	0.71

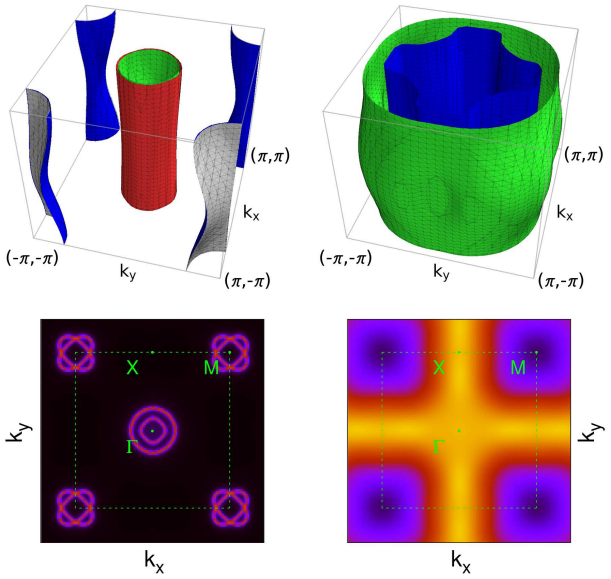

FIG. 5: Fermi surface (upper panels) and spectral weight at the Fermi level (lower panels) of tetragonal FeS as computed by DFT+DMFT for a = 6.90 a.u. (left) and a = 8.20 a.u. (right) with fixed $z_\mathrm{S} = 0.252$.

We also note that our results for the FS of the high-volume phase of FeS depend sensitively upon the lattice coordinate z_S. In particular, for the optimized value $z_\mathrm{S} = 0.127$ the electron-like pockets centered at the BZ corners become three-dimensional like, closing at a halfway from $k_z = 0$ to $k_z = \pi$. The cross-section area of the hole FS at the BZ center becomes significantly larger as compared to that in the equilibrium phase, weakly depending on k_z. In addition, we observe that the outer sheet shows concave structures at its surface, whereas the inner sheet has a cylindrical shape (see Fig. 6). The spectral weight at E_F is highly incoherent and mostly originates from the electron-like FSs at the BZ corners. Interestingly, whether or not the z_S is optimized, the lattice volume expansion results in a change of the FS topology, i.e., the Lifshitz transition in FeS. We therefore conclude that upon expansion of the lattice ("negative compression") the Lifshitz transition takes place in tetragonal FeS. The phase transition is accompanied by anomalous behavior of the crystal structure and local magnetic mo-

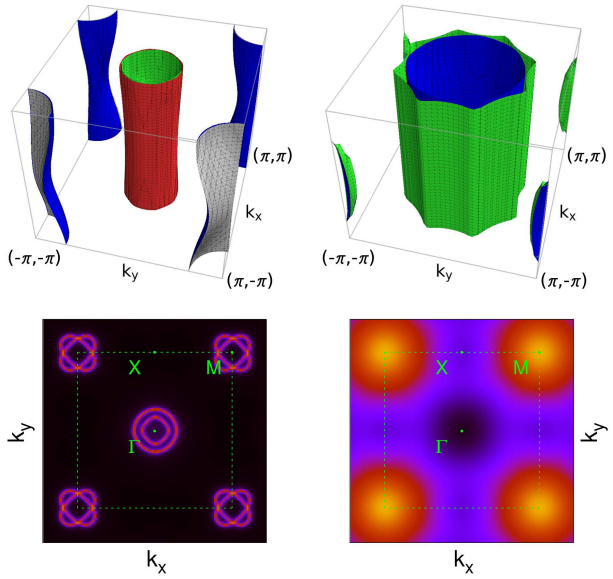

FIG. 6: Fermi surface (upper panels) and spectral weight at the Fermi level (lower panels) of tetragonal FeS as computed by DFT+DMFT for $a = 6.90$ a.u. (left) and $a = 8.60$ a.u. (right) with optimized z_S (z_S=0.247 and 0.127, respectively).

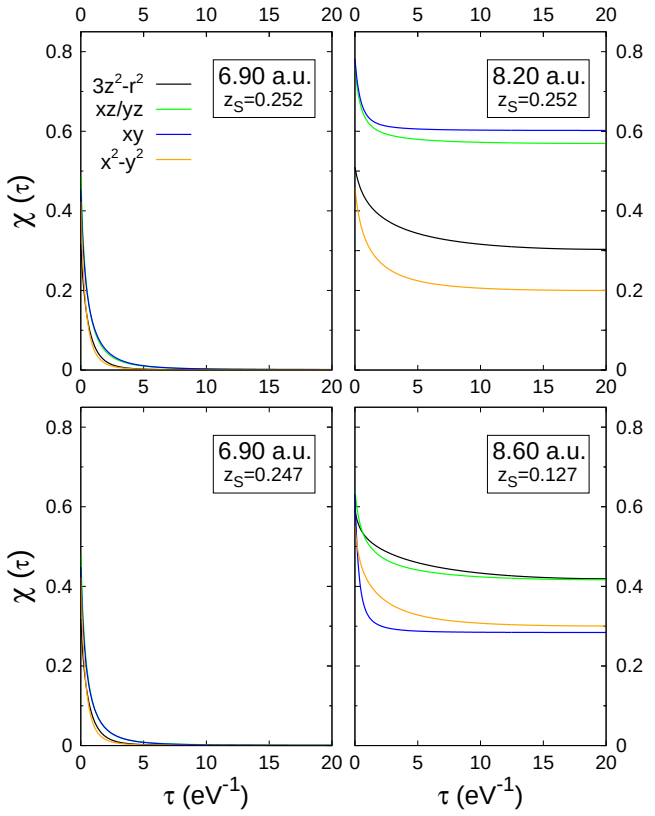

FIG. 7: Orbitally-resolved local spin correlation functions $\chi(\tau) = \langle m_z(\tau)m_z(0)\rangle$ of FeS at the equilibrium (left panels) and those in the expanded phase (right panels) as computed by DFT+DMFT at $T = 290$ K. Top row shows the result obtained with fixed internal coordinate z_S bottom row corresponds to z_S optimized within DFT+DMFT.

ments, resulting in a remarkable enhancement of electronic compressibility. Our results are therefore in line with the scenario of a correlation-induced shift of the VHS originating from the Fe t_2 orbitals at the M point towards the Fermi energy in FeSe [20–22]. The latter seems to lead to an anomalous behavior of the electronic structure, magnetism, and lattice properties of FeS upon variation of its lattice.

D. Spin susceptibility and orbital-selective local moments

We now turn to the magnetic properties of FeS and discuss our results for the spin susceptibility and orbital-selective local moments in paramagnetic FeS. In Fig. 6 we show our results for the orbital-dependent spin susceptibility $\chi(\tau) = \langle \hat{m}_z(\tau)\hat{m}_z(0)\rangle$ computed within DFT+DMFT. We found that the electronic and structural phase transition upon expansion of the lattice volume is accompanied by a significant growth of the fluctuating local magnetic moments. The transition results in a crossover from itinerant (at ambient conditions) to orbital-selective localized moment behavior (in the high-volume phase), as is seen from the spin correlation function. In fact, our calculations reveal that the expanded-volume phase exhibits an orbital-selective enhancement of localization of the Fe $3d$ electrons. Interestingly, we found that the symmetry of magnetic correlations depends sensitively on a change of the lattice parameter z_S value, whereas the overall tendency to form local moments remains the same. In particular, upon simultaneous optimization of a and z_S, we obtain that the $3z^2-r^2$ and xz/yz states in FeS show more localized behavior (to form fluctuating local moments) than that for the x^2-y^2 and xy orbitals.

To analyze the effect of lattice expansion on the symmetry and strength of magnetic fluctuations we compute the momentum-dependent static magnetic susceptibility $\chi(\mathbf{q})$. Orbital contributions of $\chi(\mathbf{q})$ along the Γ-X-M-Γ path are shown in Fig. 8. At ambient conditions, the susceptibility resembles that computed earlier for the equilibrium phase of FeSe. In particular, $\chi(\mathbf{q})$ exhibits a maximum at the M point of the tetragonal Brillouin zone, implying that leading magnetic instability at ambient pressure in FeS is due to the t_2 states, with a propagating wave vector (π, π). However, we found that unlike to FeSe the largest contribution at the M point is now originating from the xz/yz orbitals but not from the xy states as in FeSe. We also note that in the equilibrium phase of FeS the amplitude of spin fluctuations quantified by $\chi(\mathbf{q})$ is overall smaller than that in FeSe. Overall, these results suggest that there exists a crossover of magnetic correlations in Fe(Se,S) upon substituting Se with S.

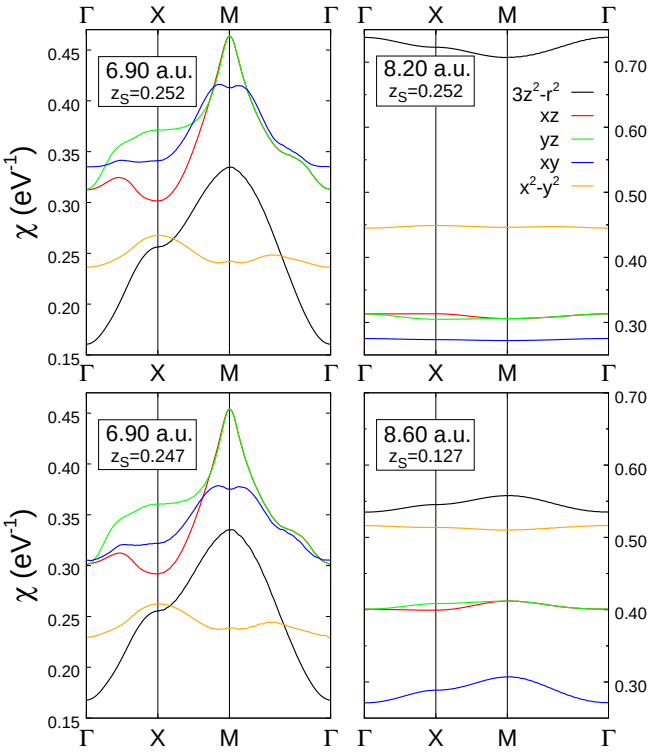

FIG. 8: Orbitally-resolved static spin susceptibility $\chi(\mathbf{q})$ of FeSe calculated by DFT+DMFT at fixed (top panels) and relaxed (bottom panels) internal coordinate z_S. Left panels correspond to the equilibrium lattice constant, right panels show the DFT+DMFT results for the expanded phase.

Our results show that expansion of the lattice volume is accompanied by a reconstruction of magnetic correlations. Thus, upon expansion of the lattice we observe an overall enhancement of $\chi(\mathbf{q})$. In the expanded-volume phase $\chi(\mathbf{q})$ has a less pronounced variance along the Γ-X-M-Γ path than that in the equilibrium phase. Moreover, the Fe e states now play a predominant role with a leading contribution originating from the $3z^2 - r^2$ orbitals. Upon expansion of the lattice, the magnetic susceptibility shows a significant damping of a peak of $\chi(\mathbf{q})$ at the M point. As a result, $\chi(\mathbf{q})$ reveals a weak feature at the Γ point, implying a possible importance of ferromagnetic fluctuations (for $z_S = 0.252$). While z_S is optimized, a leading magnetic instability has a magnetic vector (π, π), i.e., similar to that in the equilibrium phase of FeS, with a major contribution from the xy and $3z^2-r^2$ states. Overall, our results point out an anomalous sensitivity of the electronic structure and magnetic properties of FeS to the fine details of its crystals structure, e.g., to a variation of the lattice volume and lattice coordinate z_S. The latter results in a remarkable orbital-selective localization of the Fe $3d$ electrons.

IV. CONCLUSION

In conclusion, using the DFT+DMFT method we calculated the evolution of the electronic structure, magnetic properties, and the Fermi surface of FeS upon variation of its crystal structure parameters. We explore the effects of the crystal structure – changes of the lattice volume and chalcogen height z_S – on the electronic properties, orbital-dependent character and strength of magnetic correlations, and the Fermi surface topology of the tetragonal (space group P_4/nmm) FeS. Our results show a clear importance of electronic correlations for the electronic properties and structural optimization of FeS. Correlation effects reveal a strong impact on a position of the Van Hove singularity originating from the the Fe xz/yz and xy orbitals at the M point. In particular, we found that in the equilibrium structure, the QP peak associated with VHS is shifted towards the Fermi level from -0.35 to -0.23 eV. Our results suggest that the internal coordinate of sulfur, z_S, plays a key role for understanding the physical properties of FeS upon variation of the lattice volume. Upon lattice expansion, FeS is found to exhibit a structural collapsed-tetragonal to tetragonal phase transition, accompanied by a significant increase of local moments and emergence of strong orbital-selective correlations near the transition point. The phase transition is associated with a topological change of the Fermi surface (Lifshitz transition), resulting in a remarkable increase of the electronic compressibility at the transition. Our DFT+DMFT calculations exhibit an anomalous sensitivity of the electronic structure and magnetic properties of FeS to the fine details of its crystals structure, e.g., to a variation of the lattice volume and lattice coordinate z_S. Our results clearly demonstrate the crucial importance of orbital-selective correlations for a realistic description of the electronic and lattice properties of FeS, highlighting the importance of a crossover from itinerant to localized orbital-selective moment behavior of the Fe $3d$ electrons.

V. ACKNOWLEDGMENTS

Total energy calculations and analysis of magnetic correlations were performed with the support from the Russian Foundation for Basic Research according to the research project № 18-32-20076. The spectral functions, Fermi surface and the spin correlator calculations were supported by the Russian Science Foundation (Project № 19-12-00012).

[1] J. Paglione and R. L. Greene, Nat. Phys. **6**, 645 (2010); D. N. Basov and A. V. Chubukov, Nat. Phys. **7**, 272 (2011); G. R. Stewart, Rev. Mod. Phys. **83**, 1589 (2011); P. Dai, J. Hu, and E. Dagotto, Nat. Phys. **8**, 709 (2012);

Q. Si, R. Yu, and E. Abrahams, Nat. Rev. Mater. **1**, 16017 (2016).

[2] Z.-A. Ren, W. Lu, J. Yang, W. Yi, X.-L. Shen, Zheng-Cai, G.-C. Che, X.-L. Dong, L.-L. Sun, F. Zhou, and Z.-X. Zhao, Chin. Phys. Lett. **25**, 2215 (2008).

[3] S. Tan, Y. Zhang, M. Xia, Z. Ye, F. Chen, X. Xie, R. Peng, D. Xu, Q. Fan, H. Xu, J. Jiang, T. Zhang, X. Lai, T. Xiang, J. Hu, B. Xie, and D. Feng, Nat. Mater. **12**, 634 (2013).

[4] A. E. Böhmer and A. Kreisel, J. Phys.: Condens. Matter **30**, 023001 (2018).

[5] R. M. Fernandes, A. V. Chubukov, and J. Schmalian, Nat.Phys. **10**, 97 (2014).

[6] I. I. Mazin, D. J. Singh, M. D. Johannes, and M. H. Du, Phys. Rev.Lett. **101**, 057003 (2008).

[7] A. V. Chubukov, D. V. Efremov, and I. Eremin, Phys. Rev. B **78**, 134512 (2008).

[8] A. D. Christianson, E. A. Goremychkin, R. Osborn, S. Rosenkranz, M. D. Lumsden, C. D. Malliakas, I. S. Todorov, H. Claus, D. Y. Chung, M. G. Kanatzidis, R. I. Bewley, and T. Guidi; Nature (London) **456**, 930 (2008); M. D. Lumsden, A. D. Christianson, D. Parshall, M. B. Stone, S. E. Nagler, G. J. MacDougall, H. A. Mook, K. Lokshin, T. Egami, D. L. Abernathy, E. A. Goremychkin, R. Osborn, M. A. McGuire, A. S. Sefat, R. Jin, B. C. Sales, and D. Mandrus, Phys. Rev. Lett. **102**, 107005 (2009); Y. Qiu, W. Bao, Y. Zhao, C. Broholm, V. Stanev, Z. Tesanovic, Y. C. Gasparovic, S. Chang, Jin Hu, Bin Qian, Minghu Fang, and Zhiqiang Mao, Phys. Rev. Lett. **103**, 067008 (2009); M. D. Lumsden, A. D. Christianson, E. A. Goremychkin, S. E. Nagler, H. A. Mook, M. B. Stone, D. L. Abernathy, T. Guidi, G. J. MacDougall, C. de la Cruz, A. S. Sefat, M. A. McGuire, B. C. Sales, and D. Mandrus, Nat. Phys. **6**, 182 (2010); M. C. Rahn, R. A. Ewings, S. J. Sedlmaier, S. J. Clarke, and A. T. Boothroyd, Phys. Rev. B **91**, 180501(R) (2015).

[9] X. Liu, L. Zhao, S. He, J. He, D. Liu, D. Mou, B. Shen, Y. Hu, J. Huang, and X. J. Zhou, J. Phys.: Condens. Matter **27**, 183201 (2015); Y. V. Pustovit and A. A. Kordyuk, Low Temp. Phys. **42**, 995 (2016);

[10] A. I. Coldea and M. D. Watson, Annu. Rev. Condens. Matter Phys. **9**, 125 (2018);

[11] A. Kostin, P. O. Sprau, A. Kreisel, Y. X. Chong, A. E. Böhmer, P. C. Canfield, P. J. Hirschfeld, B. M. Andersen, and J. C. Séamus Davis, Nat. Mater. **17**, 869 (2018).

[12] P. O. Sprau, A. Kostin, A. Kreisel, A. E. Böhmer, V. Taufour, P. C. Canfield, S. Mukherjee, P. J. Hirschfeld, B. M. Andersen, J. C. Séamus Davis, Science **357**, 75 (2017).

[13] T.M. McQueen, A. J. Williams, P. W. Stephens, J. Tao, Y. Zhu, V. Ksenofontov, F. Casper, C. Felser and R. J. Cava, Phys. Rev. Lett. **103**, 057002 (2009).

[14] F. C. Hsu, J. Y. Luo, K. W. Yeh, T. K. Chen, T. W. Huang, P. M. Wu, Y. C. Lee, Y. L. Huang, Y. Yi. Chu, D. C. Yan and M. K. Wu, Proc. Natl. Acad. Sci. U.S.A. **105**, 14262 (2008).

[15] B. C. Sales, A. S. Sefat, M. A. McGuire, R. Y. Jin, D. Mandrus, and Y. Mozharivskyj, Phys. Rev. B **79**, 094521 (2009); V. Tsurkan, J. Deisenhofer, A. Günther, Ch. Kant, H.-A. Krug von Nidda, F. Schrettle, A. Loidl, Eur. Phys. J. B **79**, 289-299 (2011); U. R. Singh, S. C. White, S. Schmaus, V. Tsurkan, A. Loidl, J. Deisenhofer, and P. Wahl, Phys. Rev. B **88**, 155124 (2013).

[16] K. Miyoshi, K. Morishita, E. Mutou, M. Kondo, O. Seida, K. Fujiwara, J. Takeuchi, and S. Nishigori, J. Phys. Soc. Jpn. **83**, 013702 (2014).

[17] S. Medvedev, T. M. McQueen, I. A. Troyan, T. Palasyuk, M. I. Eremets, R. J. Cava, S. Naghavi, F. Casper, V. Ksenofontov, G. Wortmann, and C. Felser, Nat. Mater. **8**, 630 (2009).

[18] M. Burrard-Lucas, D. G. Free, S. J. Sedlmaier, J. D. Wright, S. J. Cassidy, Y. Hara, A. J. Corkett, T. Lancaster, P. J. Baker, S. J. Blundell, and S. J. Clarke, Nat. Mater. **12**, 15 (2013).

[19] W. Bao, Y. Qiu, Q. Huang, M. A. Green, P. Zajdel, M. R. Fitzsimmons, M. Zhernenkov, S. Chang, M. Fang, B. Qian, E. K. Vehstedt, J. Yang, H. M. Pham, L. Spinu, and Z. Q. Mao, Phys. Rev. Lett. **102**, 247001 (2009); T. J. Liu, J. Hu, B. Qian, D. Fobes, Z. Q. Mao, W. Bao, M. Reehuis, S. A. J. Kimber, K. Prokeš, S. Matas, D. N. Argyriou, A. Hiess, A. Rotaru, H. Pham, L. Spinu, Y. Qiu, V. Thampy, A. T. Savici, J. A. Rodriguez, and C. Broholm, Nat. Mater. **9**, 718 (2010); O. J. Lipscombe, G. F. Chen, C. Fang, T. G. Perring, D. L. Abernathy, A. D. Christianson, T. Egami, N. Wang, J. Hu, and P. Dai, Phys. Rev. Lett. **106**, 057004 (2011).

[20] I. Leonov, S. L. Skornyakov, V. I. Anisimov, and D. Vollhardt, Phys. Rev. Lett. **115**, 106402 (2015);

[21] S. L. Skornyakov, V. I. Anisimov, D. Vollhardt, and I. Leonov, Phys. Rev. B **96**, 035137 (2017).

[22] S. L. Skornyakov, V. I. Anisimov, D. Vollhardt, and I. Leonov, Phys. Rev. B **97**, 115165 (2018).

[23] M. D. Watson, T. K. Kim, A. A. Haghighirad, S. F. Blake, N. R. Davies, M. Hoesch, T. Wolf, and A. I. Coldea, Phys. Rev. B **92**, 121108(R) (2015).

[24] P. Reiss, M. D. Watson, T. K. Kim, A. A. Haghighirad, D. N. Woodruff, M. Bruma, S. J. Clarke, and A. I. Coldea, Phys. Rev. B **96**, 121103(R) (2017); A. I. Coldea, S. F. Blake, S. Kasahara, A. A. Haghighirad, M. D. Watson, W. Knafo, E. S. Choi, A. McCollam, P. Reiss, T. Yamashita, M. Bruma, S. C. Speller, Y. Matsuda, T. Wolf, T. Shibauchi, and A. J. Schofield, npj Quantum Materials **4**, 2 (2019).

[25] Interestingly, FeS is also known for its rich allotropic behavior under high-pressure conditions (e.g., the $P\bar{6}2c$, $Pnma$, $P2_1/a$, $Pmmn$ and $Pm\bar{3}m$ crystal structures are known). It turns out that correlation effects play an important role in the formation of the electronic and structural properties of FeS under pressure. See, e.g., A. V. Ushakov *et al.*, Phys. Rev. B **95**, 205116 (2017) and A. O. Shorikov *et al.* Phys. Rev. B **98**, 094112 (2018).

[26] X. F. Lai, H. Zhang, Y. Q. Wang, X. Wang, X. Zhang, J. H. Lin, and F. Q. Huang, J. Am. Chem. Soc. **137**, 10148 (2015); U. Pachmayr, N. Fehn, and D. Johrendt, Chem. Commun. **52**, 194 (2016).

[27] X. Lai, Y. Liu, X. Lü, S. Zhang, K. Bu, C. Jin, H. Zhang, J. Lin, and F. Huang, Sci. Rep. **6**, 31077 (2016).

[28] J. Zhang, F.-L. Liu, T.-P. Ying, N.-N. Li, Y. Xu, L.-P. He, X.-C. Hong, Y.-J. Yu, M.-X. Wang, J. Shen, W.-G. Yang, and S.-Y. Li, npj Quantum Mater. **2**, 49 (2017).

[29] M. Shimizu, N. Takemori, D. Guterding, and H. O. Jeschke Phys. Rev. Lett. **121**, 137001 (2018).

[30] A. Subedi, L. Zhang, D. J. Singh, and M. H. Du, Phys. Rev. B **78**, 134514 (2008).

[31] J. Miao, X. H. Niu, D. F. Xu, Q. Yao, Q. Y. Chen, T. P. Ying, S. Y. Li, Y. F. Fang, J. C. Zhang, S. Ideta, K. Tanaka, B. P. Xie, D. L. Feng, and Fei Chen, Phys. Rev. B **95**, 205127 (2017).

[32] C. Tresca, G. Giovannetti, M. Capone, and G. Profeta Phys. Rev. B **95**, 205117 (2017).

[33] A. Baum, A. Milosavljević, N. Lazarević, M. M. Radonjić, B. Nikolić, M. Mitschek, Z. I. Maranloo, M. Šćepanović, M. Grujić-Brojčin, N. Stojilović, M. Opel, A. Wang, C. Petrović, Z. V. Popović, and R. Hackl, Phys. Rev. B **97**, 054306 (2018).

[34] W. Metzner and D. Vollhardt, Phys. Rev. Lett. **62**, 324 (1989); A. Georges, G. Kotliar, W. Krauth, and M. J. Rozenberg, Rev. Mod. Phys. **68**, 13 (1996); V. I. Anisimov, A. I. Poteryaev, M. A. Korotin, A. O. Anokhin, and G. Kotliar, J. Phys. Condens. Matter **9**, 7359 (1997); G. Kotliar, S. Y. Savrasov, K. Haule, V. S. Oudovenko, O. Parcollet, and C. A. Marianetti, Rev. Mod. Phys. **78**, 865 (2006); A. I. Lichtenstein and M. I. Katsnelson, Phys. Rev. B **57**, 6884 (1998). J. Kuneš, I. Leonov, P. Augustinský, V. Křápek, M. Kollar, and D. Vollhardt, Eur. Phys. J. Spec. Top. **226**, 2641 (2017).

[35] I. Leonov, V. I. Anisimov, and D. Vollhardt, Phys. Rev. B **91**, 195115 (2015); I. Leonov, Phys. Rev. B **92**, 085142 (2015); I. Leonov, L. Pourovskii, A. Georges, and I. A. Abrikosov, Phys. Rev. B **94**, 155135 (2016).

[36] K. Haule, J. H. Shim, and G. Kotliar, Phys. Rev. Lett. **100**, 226402 (2008); M. Aichhorn, L. Pourovskii, V. Vildosola, M. Ferrero, O. Parcollet, T. Miyake, A. Georges, and S. Biermann, Phys. Rev. B **80**, 085101 (2009); S. L. Skornyakov, A. A. Katanin, and V. I. Anisimov, Phys. Rev. Lett. **106**, 047007 (2011); S. L. Skornyakov, V. I. Anisimov, and D. Vollhardt, Phys. Rev. B **86**, 125124 (2012); Z. P. Yin, K. Haule, and G. Kotliar, Nat. Mater. **10**, 932 (2011); Z. P. Yin, K. Haule, and G. Kotliar, Nat. Phys. **7**, 294 (2011); M. Aichhorn, L. Pourovskii, and A. Georges, Phys. Rev. B **84**, 054529 (2011); J. M. Tomczak, M. van Schilfgaarde, and G. Kotliar, Phys. Rev. Lett. **109**, 237010 (2012); Z. P. Yin, K. Haule, and G. Kotliar, Phys. Rev. B **86**, 195141 (2012); P. Werner, M. Casula, T. Miyake, F. Aryasetiawan, A. J. Millis, and S. Biermann, Nat. Phys. **8**, 331 (2012); A. Georges, L. de' Medici, and J. Mravlje, Annu. Rev. Condens. Matter Phys. **4**, 137 (2013); M. Hirayama, T. Miyake, and M. Imada, Phys. Rev. B **87**, 195144 (2013); C. Zhang, L. W. Harriger, Z. Yin, W. Lv, M. Wang, G. Tan, Y. Song, D. L. Abernathy, W. Tian, T. Egami, K. Haule, G. Kotliar, and P. Dai, Phys. Rev. Lett. **112**, 217202 (2014); A. van Roekeghem, L. Vaugier, H. Jiang, and S. Biermann, Phys. Rev. B **94**, 125147 (2016);

[37] S. L. Skornyakov, A. V. Efremov, N. A. Skorikov, M. A. Korotin, Yu. A. Izyumov, V. I. Anisimov, A. V. Kozhevnikov, and D. Vollhardt, Phys. Rev. B **80**, 092501 (2009).

[38] M. Aichhorn, S. Biermann, T. Miyake, A. Georges, and M. Imada, Phys. Rev. B **82**, 064504 (2010).

[39] P. V. Arribi and L. de' Medici, Phys. Rev. Lett. **121**, 197001 (2018).

[40] M. D. Watson, S. Backes, A. A. Haghighirad, M. Hoesch, T. K. Kim, A. I. Coldea, and R. Valentí, Phys. Rev. B **95**, 081106(R) (2017).

[41] F. Birch, Phys. Rev. **71**, 809 (1947).

[42] S. Baroni, S. de Gironcoli, A. Dal Corso, and P. Giannozzi, Rev. Mod. Phys. **73**, 515 (2001); P. Giannozzi, S. Baroni, N. Bonini, M. Calandra, R. Car *et al.*, J. Phys.:Condens. Matter **21**, 395502 (2009).

[43] N. Marzari, A. A. Mostofi, J. R. Yates, I. Souza, and D. Vanderbilt, Rev. Mod. Phys. **84**, 1419 (2012); V. I. Anisimov, D. E. Kondakov, A. V. Kozhevnikov, I. A. Nekrasov, Z. V. Pchelkina, J. W. Allen, S.-K. Mo, H.-D. Kim, P. Metcalf, S. Suga, A. Sekiyama, G. Keller, I. Leonov, X. Ren, and D. Vollhardt, Phys. Rev. B **71**, 125119 (2005); Dm. Korotin, A. V. Kozhevnikov, S. L. Skornyakov, I. Leonov, N. Binggeli, V. I. Anisimov, and G. Trimarchi, Eur. Phys. J. B **65**, 91-98 (2008); G. Trimarchi, I. Leonov, N. Binggeli, Dm. Korotin, and V. I. Anisimov, J. Phys.: Condens. Matter **20**, 135227 (2008).

[44] P. Werner, A. Comanac, L. de Medici, M. Troyer, and A. J. Millis, Phys. Rev. Lett. **97**, 076405 (2006); E. Gull, A. J. Millis, A. I. Lichtenstein, A. N. Rubtsov, M. Troyer, and P. Werner, Rev. Mod. Phys. **83**, 349 (2011).

[45] H. J. Vidberg and J. W. Serene, J. Low Temp. Phys. **29**, 179 (1977).

[46] L. Ehm, F. M. Michel, S. M. Antao, C. D. Martin, P. L. Lee, S. D. Shastri, P. J. Chupasc, and J. B. Parise, J. Appl. Cryst. **42**, 15 (2009).

[47] J. N. Millican, D. Phelan, E. L. Thomas, J. B. Leão, E. Carpenter, Solid State Commun. **149**, 707 (2009).

[48] S. Margadonna , Y. Takabayashi, M. T. McDonald, K. Kasperkiewicz, Y. Mizuguchi, Y. Takano, A. N. Fitch, E. Suard, K. Prassides, Chem. Commun. (Cambridge) **43**, 5607 (2008); M. C. Lehman, A. Llobet, K. Horigane, and D. Louca, J. Phys. Conf. Ser. **251**, 012009 (2010).

[49] Strictly speaking, our results show that the isothermal compressibility κ_T calculated within DFT+DMFT as $\kappa_T = -1/T(\partial V/\partial P)_T$ diverges at the phase transition. This is due to the fact that we neglect multiple intermediate-phase transitions when fit the total-energy result to the third-order Birch-Murnaghan equation of states separately for the low- and high-volume regions.

[50] S. L. Skornyakov, I. Leonov, V. I. Anisimov, JETP Lett. **103**(4), 265 (2016).

[51] J. Phys. Chem. Solids **72**, 562 (2011).

[52] T. Yokoya, R. Yoshida, Y. Utsumi, K. Tsubota, H. Okazaki, T. Wakita, Y. Mizuguchi, Y. Takano, T. Muro, and Y. Kato, Sci. Technol. Adv. Mater. **13**, 054403 (2012).